FRAGMENTATION OF BASALT AND SHALE PROJECTILES IN HYPERVELOCITY IMPACTS IN THE LABORATORY. J. E. Wickham-Eade[1] and M. J. Burchell[1], [1]Centre for Astronomy and Planetary Sciences, School of Physical Sciences, Ingram Building, University of Kent, Canterbury, Kent CT2 7NH, United Kingdom (jew9@kent.ac.uk).

Introduction: This work focuses on projectile survival in hypervelocity impacts. There have been studies of the projectile dating back to the 1960s, but these are less frequent than other studies. Nevertheless, projectile survival after an impact is of importance for a variety of reasons. For example: Projectile fragments have been recovered from 13 impact sites on Earth (e.g. see Table 15.1 in [1]). It has been suggested that projectile fragments can be present in central peaks in lunar impact craters [2]. The dark material on the surface of Vesta is likely to come from impactors [3]. Non-indigenous materials have been found on the Moon e.g. [4] and so on. Indeed the sub-surface regions at man-made impact sites should also contain impactor material (e.g. the crater on comet 9P/Tempel-1 arising from the Deep Impact mission [5-6]).

Laboratory studies of impactor survival do exist. There are examples such as those of [6-9]. As well as size distributions of fragments, there are reports of analyses of recovered fragments to see if the impact processed their organic content, with particular relevance to astrobiology, e.g. [10-11]. It is no surprise therefore that more studies are now appearing on projectile fragment survival, including [12-13].

Accordingly, here we report on the survival of basalt and shale projectiles fired into water at speeds up to 6 km s^{-1}. In this present work we focus on the fragment size distribution and its evolution vs. impact speed and peak shock pressure.

Method: We used the Univ. of Kent two stage light gas gun [14] to fire 1.5 mm cubes of basalt and shale into bags of water. The impacts studied were at speeds between 0.52 and 6.02 km s^{-1} for basalt and, so far, 0.95, 3.12 and 4.64 km s^{-1} for shale. The water was filtered after the impact to extract the projectile fragments. After extraction, the samples were imaged in a SEM (Hitachi S3400N) and automated software was used to find and size the individual fragments; see Fig. 1 for an example. We can extract and measure fragments down to around 10 μm in size and can find over 100,000 fragments in the higher speed shots. As a check, one sample was measured directly on the SEM by the user to confirm the accuracy of the software method.

We use the Planar Impact Approximation [15] to find peak shock pressures in each impact. This requires a linear shock wave speed relation of the form U = C + Su, with values for C and S for both projectile and target materials. From [15] we take for basalt: C = 2.60 km s^{-1}, S = 1.62 and density 2860 kg m^{-3}, for water, the equivalent values were 2.39 km s^{-1}, 1.33 and 997.9 kg m^{-3} and for shale we used 2.30 km s^{-1}, 1.61 and 2545 kg m^{-3} taken from [16].

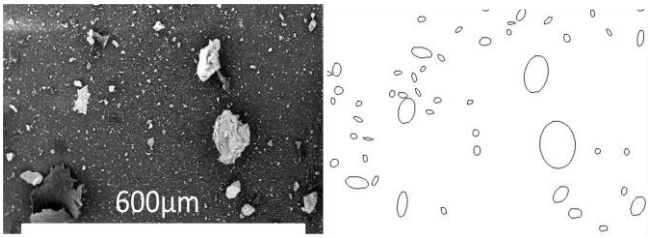

Fig. 1. SEM field of view for fragments at 3.04 km s^{-1} and software oval fit.

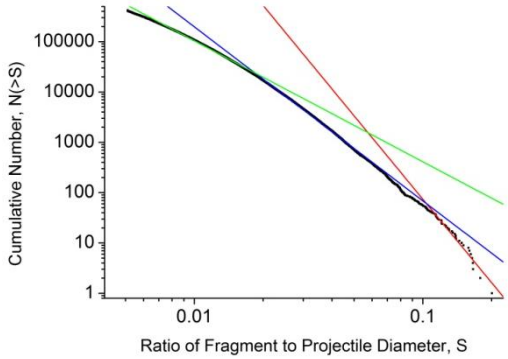

Fig. 2. Example fragment size distributions (FSD) for 0.96 km s^{-1}. The red fit is for large fragments, blue for medium and green for small.

Results: In Fig. 2, we show an example fragment size distribution (normalised to the original projectile diameter) for the impact at 0.96 km s^{-1}. We have fitted the cumulative size distributions with power laws of the form $N(>S) = aS^b$, where N is the number of fragments greater than a given size S. A single power b does not fit the entire size range of fragments recovered from a single shot and so we make 3 fits to each distribution at small, medium and large (normalised) fragment sizes. There is usually a steeper slope (larger b value) at larger fragment sizes, with a smaller slope (lower b value) at smaller sizes. b ranges for basalt and shale from: Small sizes -2.4 to -3.6 and -1.7 to -3.6, Intermediate Sizes -3.5 to -4.2 and -2.9 to -4.3 and at the Largest Sizes -4.4 to -6 and -0.8 to -11 respectively.

The behavior of the fragment size at the very largest sizes depends sharply on impact speed. At the lower speeds the first few largest fragments form a concave shape on the cumulative size distribution in log-log space. This flattens out at an intermediate

speed (3 km s^{-1}, 10.5 GPa) and then becomes convex at higher speeds. This is suggestive of the behavior of the similar cumulative size distributions for fragmented *targets* as they pass from the just disrupted to the heavily disrupted regimes (e.g. see [17-18]). This behaviour also appears to be seen in the shale results.

We used the ratio of the largest axis (a) and an orthogonal axis (b) to characterise each fragment shape. We find that the average mean value over all sizes and speeds of b/a for basalt and shale is 0.60 ± 0.19 and 0.64 ± 0.17 respectively.

We have also estimated the total surviving mass percentage we extract after each impact. This is shown in Fig. 3 vs. peak shock pressure as found by the PIA. We see an initially rapid drop in the surviving mass but this then flattens off at higher speeds and pressures. Given that, due to the small size of the grains, there is not much mass in the very fine size fraction below 10 μm where our sensitivity falls off, the missing mass is likely carried away from the target (by water lost during the impact back along the impact direction where our target holder was not sealed to allow entrance of the projectile) as suggested for example in [19]. Or increasingly amounts of the projectile start to be vaporized. It appears that after our first three shots shale has a similar surviving mass percentage to basalt at low shock pressures, however, at higher shock pressures it has a higher surviving mass percentage.

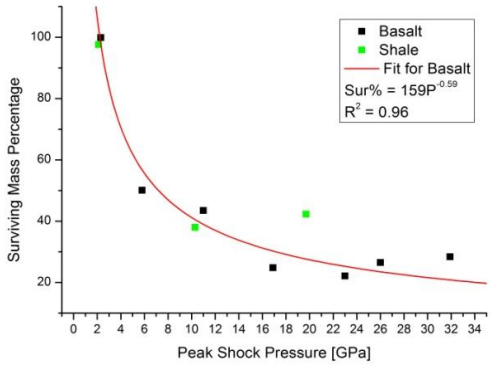

Fig. 3. Surviving mass percentage vs. peak shock pressure.

We have also looked at the relationship of the largest fragment mass ratio $m_{L,p}/M_p$ with the projectile impact energy density Q_p, as suggested in the literature [20][21]. This plotted with previous data [20][21] suggests that over the shot regime there is a change in slope past ~1 km s^{-1}, see Fig. 4. However, the latter part of the shot regime agrees with data of basalt projectiles impacting at non-normal incidence [20]. We calculate that the energy density at which catastrophic disruption of the basalt projectile occurs is (25.1 ± 1.9) x10^4 J kg^{-1}.

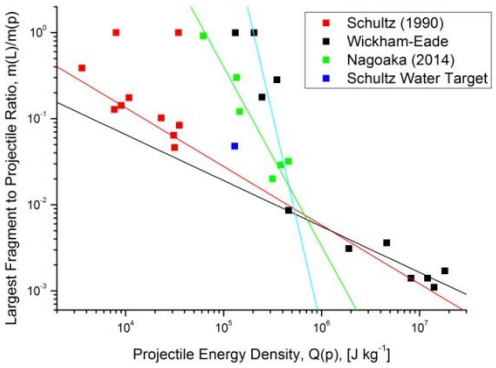

Fig. 4. Largest fragment mass ratio $m_{L,p}/M_p$ vs. projectile impact energy density Q_p.

Conclusions: We have conducted a detailed set of measurements of the fragment size distribution for impacts of basalt and shale on to water in the speed range 0.52 to 6.02 km s^{-1} and 0.95 to 4.64 km s^{-1}, which corresponds to peak shock pressures of 1.1 to 31.9 GPa and 2.1 to 19.7 GPa respectively. The fragment size distribution changes with increasing impact speed, with fewer large fragments in the higher speed shots. However, even at the higher speeds there is significant retention of the projectile material in the target.

Preliminary results for shale indicate a higher disruptive energy and a higher surviving mass fraction at high shock pressures than for basalt.

References: [1] Goderis S. et al. (2013) Chapter 15, 223 – 239, in: *Impact cratering processes and products*. Edited by G.R. Osinski and E. Pierazzo, pub. Wiley-Blackwell. [2] Yue Z. et al. (2013) *Nature Geoscience, 6*, 435–437. [3] Reddy V. et al. (2012) *Icarus, 221(2)*, 544–559. [4] Joy K.H. et al., (2012) *Science, 336(6087)*, 1426–1429. [5] Schultz P.H. et al. (2013) *Icarus, 222*, 502–515. [6] McDermott et al., (2016) Icarus, doi:10.1016/j.icarus.2015.12.037 [7] Schultz P.H. and Gault D.E. (1984) *LPSC XV*, Abstract #730. [8] Hernandez V.S. et al (2006) *IJIE, 32*, 1981–999. [9] Kenkmann T. et al. (2013) *MAPS, 48(1)*, 150–164. [10] Parnell J. et al. (2010) *MAPS, 45*, 1340–1358. [11] Burchell et al. (2014) *Astrobiology, 14(6)*, 473–485. [12] Daly R.T & Schultz P.H. (2015) *GRL, 42*. [13] Daly R.T. & Schultz P.H. (2016) *Icarus, 264*, 9-19. [14] Burchell M. et al. (1999) *Meas. Sci. Tech., 10(1)*, 41–50. [15] Melosh H.J. (1989) *Impact cratering: a geologic process*. OUP. [16] Ahrens J.T. and Johnson M.L. (1995) Chapter 4, 35-44, in: *Rock physics and phase relations*. AGU. [17] Durda D.D. et al. (2007) *Icarus, 186*, 498–516. [18] Leliwa-Kopystynski et al. (2010) *MAPS, 44*, 1929–1935. [19] Burchell M.J. et al. (2012) *MAPS, 47*, 671– 683. [20] Schultz P.H. and Gault D.E. (1990) *Geo. Soc. America, Special Paper 247*. [21] Nagaoka H. et al. (2014) *MAPS, 49*, 69–79.